IEEE Access
Multidisciplinary ⁝ Rapid Review ⁝ Open Access Journal

Received 9 April 2024, accepted 8 May 2024, date of publication 16 May 2024, date of current version 29 May 2024.

Digital Object Identifier 10.1109/ACCESS.2024.3401826

RESEARCH ARTICLE

LTCC Differential-Fed Broadband High-Gain and Narrow-Beam Planar Aperture Antenna for AiP Millimeter-Wave-Applications

MUHAMMAD ADNAN[1], TAEYONG JEONG[1], JONGJIN PARK[2],
YOUNGOO YANG[1], (Senior Member, IEEE),
KANG-YOON LEE[1], (Senior Member, IEEE),
AND KEUM CHEOL HWANG[1], (Senior Member, IEEE)
[1]Department of Electrical and Computer Engineering, Sungkyunkwan University, Suwon 16419, Republic of Korea
[2]AOT Korea Company Ltd., Seoul 05804, Republic of Korea

Corresponding author: Keum Cheol Hwang (khwang@skku.edu)

This work was supported by the Project for Collabo Research and Development between Industry, University, and Research Institute funded by Korea Ministry of Small and Medium-sized Enterprises (SMEs) and Startups, in 2023, under Grant RS-2023-00224960.

ABSTRACT The article presents a differentially excited low temperature co-fired ceramics (LTCC) based miniaturized planar aperture antenna, distinguished for its high gain and narrow-beam wideband characteristics, tailored specifically for mm-Wave antenna-in-package (AiP) applications. The proposed antenna comprises a stepped-cut patch element excited differentially and enclosed within an open cavity formed by metallized vias. Four tuning stubs are symmetrically incorporated into the stepped-cut patch element, and two pairs of shorting vias are used to ground it, improving overall impedance and gain bandwidth. Rectangular-shaped parasitic strips, strategically positioned outside the open cavity in a symmetrical arrangement, significantly narrow the main beam along two principal cutting planes, thereby enhancing broadside gain across the entire frequency band of operation. To validate the proposed design, a miniaturized and low loss differential feeding network was designed using the same LTCC technology and seamlessly integrated into the underside of the prototype antenna. According to measured results, the fabricated prototype exhibit −10 dB impedance bandwidth of 20.97 % (56.55–69.8 GHz), and the realized gain is higher than 10.01 dBi with a peak gain of 12.36 dBi at 63 GHz. Moreover, the radiation pattern of the proposed design is perfectly symmetrical, boasting a half-power beamwidth less than 40° along both the planes across the entire operating band.

INDEX TERMS Low temperature co-fired ceramics (LTCC), differentially-fed planar aperture antenna, millimeter-wave (mm-Wave), substrate-integrated-waveguide (SIW), parasitic strips, tuning stubs.

I. INTRODUCTION

The emergence of new 60 GHz wireless products is thrilling, not solely for meeting the high-speed wireless access needs of consumers, but also due to their potential deployment worldwide, facilitated by harmonized global spectrum regulations [1]. The rise of this technology facilitates the wireless transmission of high-definition video and rapid file transfer without compression. These advancements necessitate cost-effective, compact systems that integrate radio-frequency integrated circuits (RFICs), passive components, antennas, switches, and high-performance interconnects [2]. In such systems, antennas must avoid intercepting multipath signals and concentrate transmission power in a specific direction. Utilizing a narrow beam antenna reduces interference with signals from other directions, thus improving signal-to-noise ratio (SNR), which is particularly advantageous for line-of-sight (LOS) communication deployments. Furthermore, by maximizing the effective use of available spectrum resources, narrow beam antennas enhance

The associate editor coordinating the review of this manuscript and approving it for publication was Ladislau Matekovits.

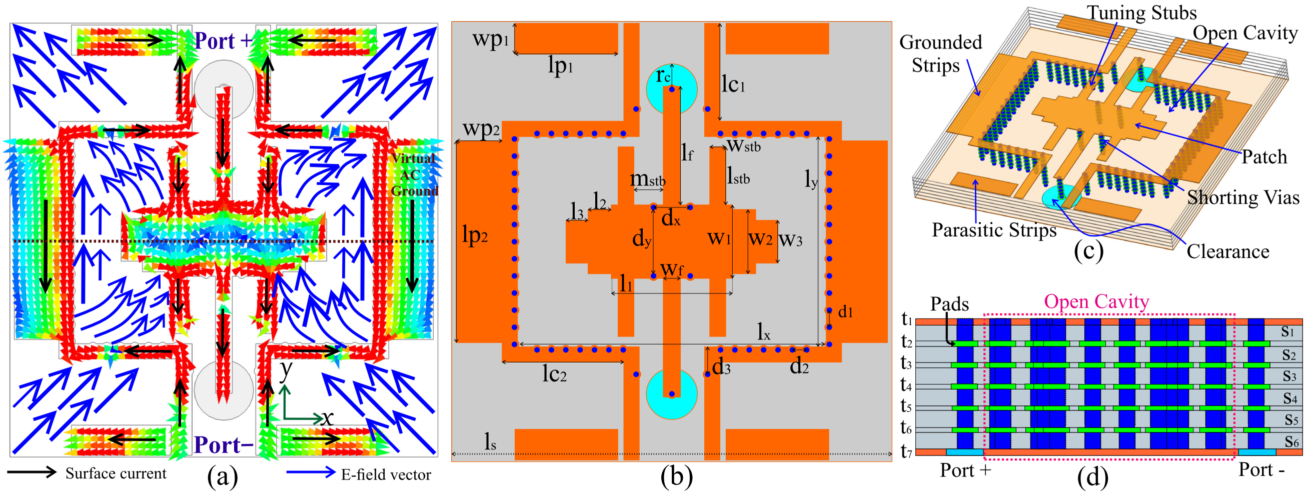

FIGURE 1. **Proposed differential fed antenna. (a) Working principle. (b) Top view. (c) 3D view. (d) Side view. ($l_s = 7.2$, $l_x = 5.02$, $l_y = 3.44$, $l_{c1} = 1.6$, $l_{c2} = 1.99$, $l_{p1} = 3.3$, $l_{p2} = 1.68$, $w_{p1} = 0.75$, $w_{p2} = 0.5$, $d_1 = 0.28$, $d_2 = 0.235$, $d_3 = 0.45$, $l_1 = 1.98$, $l_2 = 0.38$, $l_3 = 0.36$, $w_1 = 1.2$, $w_2 = 1.05$, $w_3 = 0.7$, $r_c = 0.5$, $l_f = 1.94$, $w_f = 0.28$, $d_x = 0.6$, $d_y = 1.12$, $l_{stb} = 0.95$, $w_{stb} = 0.26$, $m_{stb} = 0.48$) (Units = mm).**

overall spectral efficiency, allowing more users to be served within the same frequency bands. It's important to note that a high-gain antenna doesn't guarantee a narrow main beam in both planes. For example, substrate-integrated-waveguide (SIW) based wideband H-plane horn antenna [3], [4] demonstrates a narrower main beam along the H-plane but retains a wider main beam along E-plane, allowing room for interference from multipath signals across the E-plane.

Researchers worldwide have proposed numerous aperture antennas for antenna-in-package (AiP) mm-Wave applications, each offering unique characteristics. For instance, a PCB-based planar aperture antenna [5] achieves a remarkable –15 dB impedance bandwidth covering 21.5% (56.2-69.7 GHz), with a broadside peak gain of 15.3 dBi and a half-power beamwidth (HPBW) spanning 20° to 30°. A 2 × 2 magnetoelectric dipole array [6], enclosed within a rectangular cavity, achieves an impressive impedance bandwidth of 29.2% from 52.6 to 70.6 GHz, with a gain ranging from 10.9 to 13.7 dBi and a half-power beamwidth ranging from 40° to 50°. Despite their excellent performance in terms of impedance and gain bandwidths, extending these designs to an array configuration is hindered by the complexity of the feeding network. Additionally, the designs are not the most compact. In reference [7], a single-layered broadband magnetoelectric dipole antenna demonstrates a –10 dB impedance bandwidth from 57 to 71 GHz, achieving a realized gain of 9.1 dBi, accompanied by a half-power beamwidth ranging from 50° to 60°. However, the E-plane radiation pattern displays asymmetry and tilt, and there is a lack of compatibility with differential microwave circuits. Another promising approach is demonstrated in [8], where a low temperature co-fired ceramics (LTCC) based single-ended fed planar aperture antenna exhibits a –8 dB impedance bandwidth from 57 GHz to 64 GHz, with a half-power beamwidth ranging 40° to 50° and a peak gain of 11.5 dBi. While this design readily extends to an array for high gain, integrating it into differential mm-Wave circuits proves infeasible. In recent work [9], Liao and Xue introduced a dual-polarized planar aperture antenna with LTCC technology for a 60 GHz CMOS differential transceiver chip, featuring a –10 dB impedance bandwidth (57-64 GHz), a peak gain of approximately 12 dBi, and a half-power beamwidth spanning 40° to 50° for both polarizations. However, extending the design to an array configuration is challenging due to the complexity of the required differential feeding network. In summary, the quest to design a low-profile antenna capable of achieving extremely narrow beamwidths in both planes, along with high gain and broad impedance bandwidth, presents significant challenges.

In this paper, a miniaturized LTCC-based broadband planar aperture antenna is proposed, incorporating differential feeding, and distinguished by its high gain and exceptionally narrow half-power beamwidth along both planes. The antenna composed of a rectangular opening cavity that encloses a stub-integrated stepped-cut patch element. The element is differentially excited by two probes and grounded through four symmetrical vias, complemented by symmetrical parasitic strips positioned outside the cavity to narrow the main beam in both planes and enhance gain. The antenna design is optimized using ANSOFT High-Frequency Structure Simulator (HFSS) to minimize half-power beamwidth along both planes and enhance gain with in the interested frequency band. Experimental validation demonstrates an impressive impedance bandwidth of 20.97% (56.55 to 69.80 GHz) and realized gain between 10.01 dBi to 12.36 dBi, with a half-power beamwidth less than 40° along the two principal cutting planes. These achievements position the proposed antenna as a strong contender for mm-Wave applications, particularly in antenna-in-package configurations.

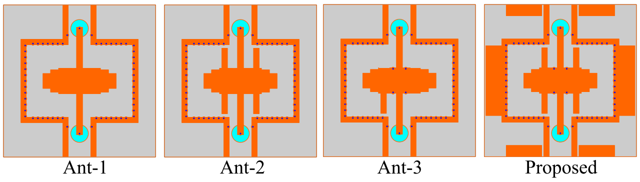

FIGURE 2. Design process of proposed antenna.

This paper is organized as follows: Section II presents the antenna's configuration, design evolution, and operating principle. Section III conducts pivotal parametric studies. Section IV describes the design process for the differential feeding network. In Section V, results from simulations and measurements of the fabricated antenna prototype with the differential feeding network are presented. Finally, Section VI encapsulates the conclusions.

II. ANTENNA DESIGN

A. ANTENNA CONFIGURATION AND DESIGN EVOLUTION

The proposed differentially-fed planar antenna element, as depicted in Figure 1(b), comprises 6 LTCC layers and 7 metal layers, as illustrated in Figure 1(d). Ferro A6M, with a dielectric constant of 5.9 and a loss tangent of 0.002, serves as the dielectric material in the proposed design, with each LTCC layer measuring 0.1 mm in thickness and 7.2 mm in width. The proposed antenna design features an open metallized cavity as the antenna aperture, activated by a differentially-fed stepped-cut patch element. Strips making the open cavity peripherals are grounded via 0.1 mm diameter through vias, traversing multiple layers (S_1-S_6) as shown in Figure1(d). To ensure through connection among vias on each layer, 0.15 mm diameter pads are utilized. At 0.6 mm in height, the open cavity nearly matches a quarter of the dielectric wavelength at 57 GHz, which guarantees the maximum amplitude of the E-field of the aperture.

Figure 2 shows the evolutionary process of the proposed antenna design. Initially, the stepped-cut patch element stimulates the cavity as can be seen in Figure 2 (Ant-1). The cavity's sidewalls effectively suppress surface waves, reducing the beamwidth and side-lobe radiation levels, thereby enhancing the broadside gain. Satisfactory performance is observed at 66 GHz; however, at lower frequencies of the operating band, broader main beams lead to decreased gain, and an undesirable radiation null around 62.5 GHz is evident due to poor impedance matching, as illustrated in Figure 3. Hence, additional components and techniques are necessary to enhance proposed antenna performance, especially at lower frequencies.

In the subsequent phase, tuning stubs are integrated into the stepped-cut patch element, as illustrated in Figure 2 (Ant-2). As depicted in Figure 3, these stubs notably improve impedance matching from 56 to 63 GHz, consequently enhancing the realized gain by perturbing the field distribution and achieving a broadside radiation pattern, yet the half-power beamwidth along the E-plane is increased.

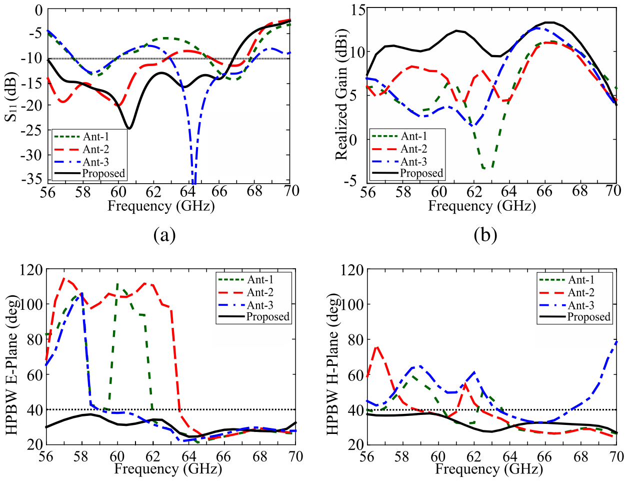

(a) (b)

(c) (d)

FIGURE 3. Comparison of the simulated results for Ant-1 to Proposed. (a) $|S_{11}|$ (b) Realized Gain (c) Half-power beamwidth along the E-Plane (*yz*-plane). (d) Half-power beamwidth along the H-Plane (*xz*-plane).

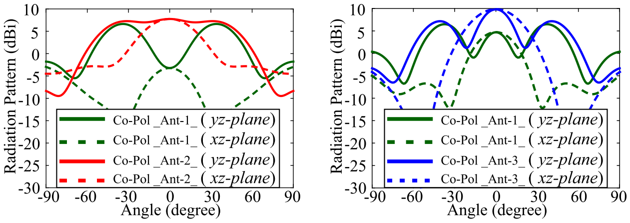

(a) (b)

FIGURE 4. Comparison of the simulated co-polarized radiation pattern along the E-plane (*yz*-plane) and H-plane (*xz*-plane) at (a) 62.5 GHz for Ant-1 and Ant-2 and (b) 64 GHz for Ant-1 and Ant-3.

In Figure 4(a), simulated co-polarized radiation patterns along the E-plane and H-plane are presented both for Ant-1 and Ant-2 at 62.5 GHz. It is evident that the radiation null has been eliminated, and a main lobe is achieved in the broadside direction. Moreover, they induce unidirectional surface currents, reducing the cross-polarization level, notably at the low-frequency range of the operating band.

In the third step, the stepped-cut patch element is shorted to the ground using four symmetrical shorting vias, as illustrated in Figure 2 (Ant-3). This characteristic transforms the proposed antenna into a quasi magnetoelectric dipole antenna, wherein the horizontal stepped-cut patch element functions as an electric dipole and the shorting vias act as a magnetic dipole. For frequencies from 62.5 to 68 GHz, the current on the shorting vias reaches maximum intensity, thus effectively working as a magnetic dipole. As observed in Figure 3, this notably improves the impedance matching and consequently enhances the realized gain from 62.5 to 68 GHz, reinforcing the E-field distribution within the cavity. Additionally, they significantly reduce the half-power beamwidth along the E-plane from 59 to 62 GHz. Figure 4(b) compares the co-polarized radiation pattern for Ant-1 and Ant-3 at 64 GHz along both the principal cutting planes.

Subsequently, a pair of parasitic strips is positioned outside the open cavity along both the H-plane (i.e., xz-plane) and E-plane (i.e., yz-plane), as depicted in Figure 2 (Proposed). The H-plane strips interconnect with the cavity's periphery, while those in the E-plane are excited by the external field. The surface current distribution on these parasitic strips, along with the grounded cavity strips, enhances gain by expanding the antenna's physical aperture. Their alignment ensures a consistent E-field direction both inside and outside the cavity, thereby reducing the half-power beamwidth along both the principal cutting plane and increasing realized gain, particularly from 56 to 63 GHz, as can be seen in Figure 3.

In the context of our antenna design, the decision not to extend the open cavity sidewall vias beyond the signal probe along the E-plane (yz-plane) and to implement a stepped-cut patch element results in improved impedance matching and a narrower half-power beamwidth, thereby enhancing gain. Conversely, extending the sidewall vias beyond the signal probe and opting for a simple patch configuration leads to significant energy reflection, ultimately widening the half-power beamwidth and consequently reducing realized gain. The structural attributes of the opening cavity, including the dimensions and shape of the stepped-cut patch element, play a pivotal role in managing field distribution across varying frequencies. Thus, the proposed planar aperture antenna maintains consistent impedance matching, a narrower half-power beamwidth, excellent realized gain, and a stable radiation pattern across an extensive frequency range.

The optimized prototype features an impressive impedance bandwidth of 17.26% (55.95–66.52 GHz) with a return loss exceeding 10 dB. It maintains a half-power beamwidth of less than 40° along both the H-plane and E-plane, as well as a broadside realized gain of over 10.56 dBi and near-zero cross-polarization. Remarkably, it achieves a peak gain of 13.28 dBi at 66 GHz, demonstrating outstanding performance. Figure 1(b) depicts the prototype along with all its optimized geometrical parameters

The aperture efficiency of an antenna can be calculated using the formula provided in reference [10].

$$\epsilon_{ap} = \frac{\lambda^2 G}{4\pi A_p}$$

where λ, G, and A_p represent the operating wavelength, gain and antenna's physical aperture, respectively. By considering solely the cavity area $l_x \times l_y$ as the physical aperture of the antenna, the computed aperture efficiency at 66 GHz exceeds 160%, which clearly contradicts physical laws. This discrepancy suggests that the real physical aperture extends beyond the area which is solely occupied by the open cavity, as the field surrounding the open cavity edges and on the parasitic strips also contribute to radiation and antenna gain. When considering the substrate area $l_s \times l_s$ as the antenna's physical aperture, the computed aperture efficiency at 66 GHz decrease to 67.47%. Seeing that the exact determination of the physical aperture for the proposed design remains uncertain, it is reasonable to infer that its aperture efficiency is at least 67.47%, given that the antenna's aperture is unlikely to exceed the ground size.

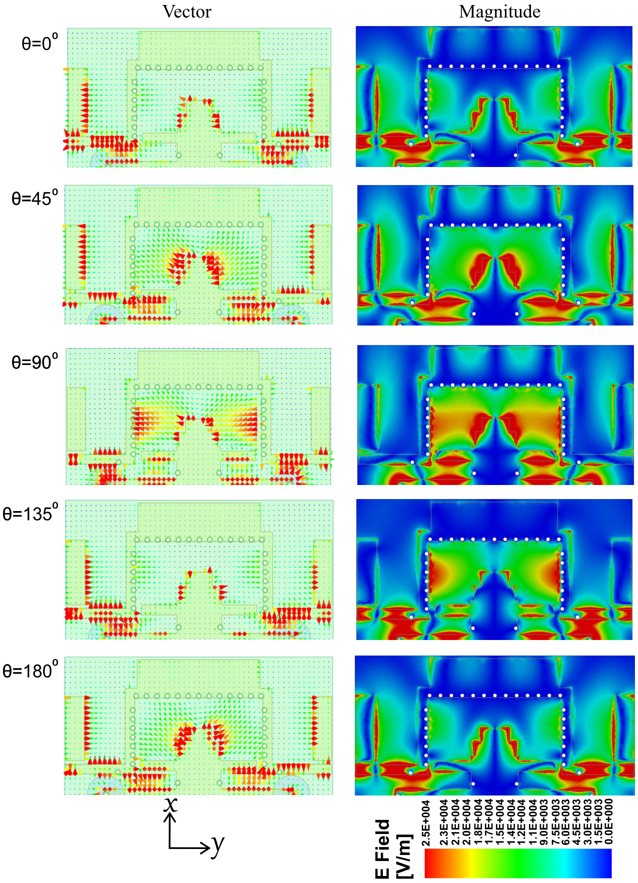

FIGURE 5. ***E*-field distribution for various phases on the proposed antenna's surface at 60 GHz. Regarding symmetrical boundaries, only half of the structure is displayed.**

B. OPERATING PRINCIPLE

Contrary to conventional patch antennas, cavity-backed patch antennas [11] and the former aperture antennas [12], [13], [14], [15], the proposed aperture antenna functions on a distinctive principle. For the proposed aperture antenna, the cavity's dimensions are larger than one wavelength, hence featuring a substantial physical aperture, which is one of the most essential factors for achieving high gain in aperture antennas. Due to the differential feeding, energy flows into the open cavity via signal probes from the differential ports and propagates along the patch element in the $\pm x$ direction in a traveling waveform. The energy across the patch yields uniform E-field distributions, illuminating the aperture, which, notably, do not manifest as resonant modes within the cavity. Furthermore, the symmetrical geometry and excitation lead to the formation of a virtual AC ground parallel to the H-plane across the center of the antenna, restricting energy passage. As the proposed aperture antenna operates independently of resonance and utilizes the physical aperture as the main energy pathway, so it achieves high gain, narrower half-power beamwidth, and potential wide impedance bandwidth.

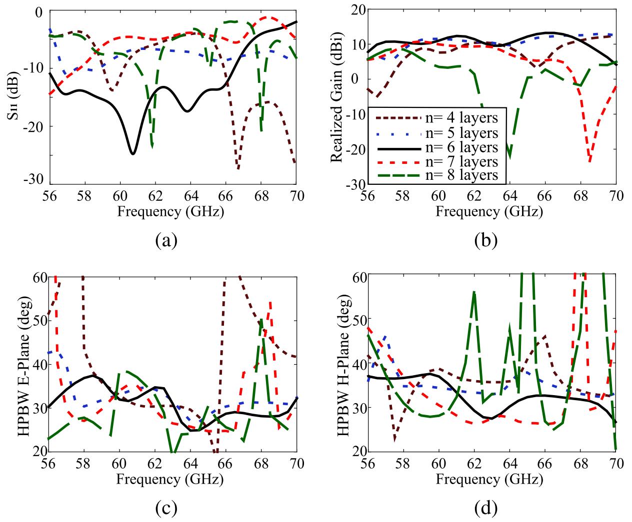

FIGURE 6. Simulated $|S_{11}|$, realized gain and half-power beamwidth both along the E-Plane and H-Plane verses the frequency for different number of substrate layers (n).

For a deeper understanding of the proposed antenna's operation, Figure 5 illustrates the simulated E-field distribution on its surface at 60 GHz, showcasing different phases. Observing the E-field magnitude, a symmetrical and uniform electric field distribution is observed both within the antenna's physical aperture and on the dielectric margins outside the open cavity. The E-field strength remains consistent along the edges of the stepped-cut patch element and the parasitic strips. Moreover, there is a clear concentration of uniform E-field distribution. between the tuning stub and feeding line. In this figure, we can also observe a gradual weakening of the surface vector E-field distributions along the $-y$-direction. Interestingly, as the phase progresses from 0° to 180°, there's a complete reversal in their orientation. This phenomenon strongly indicates excellent linear polarization, precisely as we anticipated. Comprehending this observation is crucial for analyzing the behavior of the antenna, since it reflects the magnitude as well as the orientation of the electromagnetic fields, which are necessary for maximizing its efficiency.

III. PARAMETRIC STUDIES

A parametric study was conducted to further investigate the proposed antenna design principle and analyze how adjustments in size parameters are made to achieve objectives such as wide impedance bandwidth, narrower half-power beamwidth, and high realized gain. Several critical parameters, including the number of substrate layers (n), open cavity size (l_x,l_y), length and width of the parasitic strips (l_{p1},w_{p1}), and tuning stubs (l_{stb},w_{stb}) are selected for parametric studies. During the investigation of a specific parameter, the remaining parameters are held constant at their optimal values as provided in the captions of Figure 1.

A. NUMBER OF SUBSTRATE LAYERS

Figure 6 illustrates how varying the number of LTCC substrate layers (ranging from $n = 4$ to $n = 8$) affects the reflection coefficient, realized gain, and half-power beamwidth performance of the proposed antenna. As shown, the number of substrate layers significantly influences the impedance matching, realized gain, and half-power beamwidth values along both the planes across the entire operating bandwidth. When the number of substrate layers is decreased, impedance matching deteriorates, peak gain decreases, the half-power beamwidth value increases, and the operating bandwidth shifts to higher frequencies. Consequently, the antenna achieves a broad overlapping impedance/realized gain bandwidth and the narrowest half-power beamwidth along both the planes within the operating frequency band when the number of substrate layers are $n = 6$. Varying the number of LTCC substrate layers from its optimal value leads to performance degradation of the antenna at the desired frequency. This is primarily due to its direct influence on the amplitude of the E-field aperture, which is maximized when the antenna height approximates one-quarter of the dielectric wavelength at the target frequency.

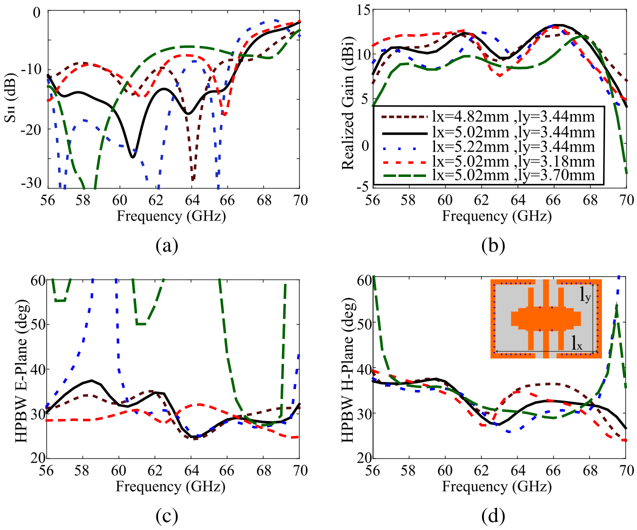

FIGURE 7. Simulated $|S_{11}|$, realized gain and half-power beamwidth both along the E-Plane and H-Plane verses the frequency for different open cavity sizes(l_x and l_y).

B. OPEN CAVITY SIZE

Figure 7 depicts $|S_{11}|$, broadside realized gain, and half-power beamwidth corresponding to different dimensions of l_x and l_y. As l_x increases from 5.02 mm to 5.22 mm, impedance matching improves for frequencies from 56 to 62 GHz. However, broadside realized gain decreases, and the half-power beamwidth value increases along the E-plane (i.e., yz-plane) for frequencies from 57 to 61 GHz, along with the shifts in the operating band to lower frequencies. Likewise, increasing l_y from 3.44 mm to 3.70 mm degrades antenna performance significantly, leading to deteriorated impedance matching for frequencies from 61 to 66 GHz, reduced realized gain, and increased half-power beamwidth value along the E-plane across the

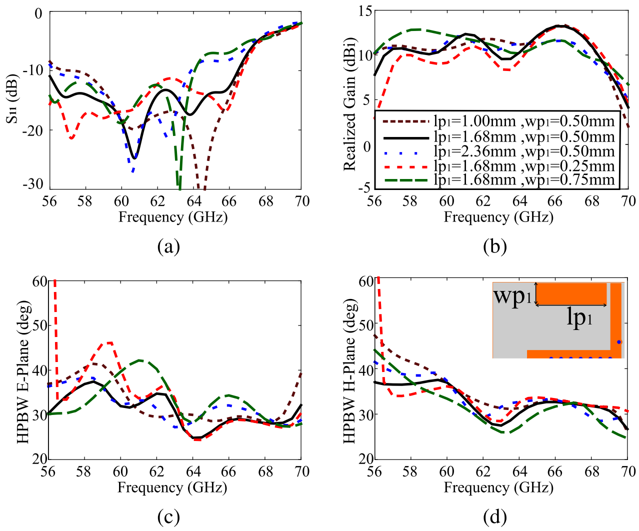

(a) (b) (c) (d)

FIGURE 8. **Simulated $|S_{11}|$, realized gain and half-power beamwidth both along the E-Plane and H-Plane verses the frequency for different parasitic strip sizes(l_{p1} and w_{p1}).**

entire operating band. Thus, $l_x = 5.02$ mm and $l_y = 3.44$ mm are chosen as the optimal values for achieving the widest overlapping impedance/realized gain bandwidth and the narrowest half-power beamwidth along both planes.

C. PARASITIC STRIPS

In Figure 8, we observe the influence of length l_{p1} and width w_{p1} of the parasitic strips on $|S_{11}|$, broadside realized gain, and half-power beamwidth for the proposed antenna design. As l_{p1} decreases from 1.68 mm to 1.0 mm, $|S_{11}|$ notably improves for frequencies from 61 to 66 GHz, yet it exceeds the -10 dB impedance bandwidth around 57 GHz. Additionally, broadside realized gain increases for frequencies from 62 to 65 GHz; however, the half-power beamwidth exceeds 40° at lower frequencies within the operational bandwidth.While increasing l_{p1} beyond the optimal value, impedance matching deteriorates, resulting in reduced realized gain for the frequency range of 63 to 66 GHz. Comparatively, the width w_{p1} of the parasitic strips exhibits a more substantial impact on the antenna's performance than the length l_{p1}. Reducing the w_{p1} value to 0.25 mm improves impedance matching, although this comes with the drawback of reduced realized gain, with the half-power beamwidth exceeding 40° along the E-plane (i.e., yz-plane) around 57 GHz. Conversely, an increase in w_{p1} value from 0.5 mm to 0.75 mm enhances $|S_{11}|$ and realized gain for frequencies ranging from 56 to 63 GHz. However, from 63 to 67 GHz, this leads to deterioration in matching and a reduction in realized gain. Furthermore, the half-power beamwidth value exceeds 40° along the E-plane (i.e., yz-plane) around 63 GHz. Therefore, to achieve a broad overlapping impedance/realized gain bandwidth and a half-power beamwidth value less than 40° along both the planes, the values of l_{p1} and w_{p1} are finally set to 1.68 mm and 0.5 mm, respectively.

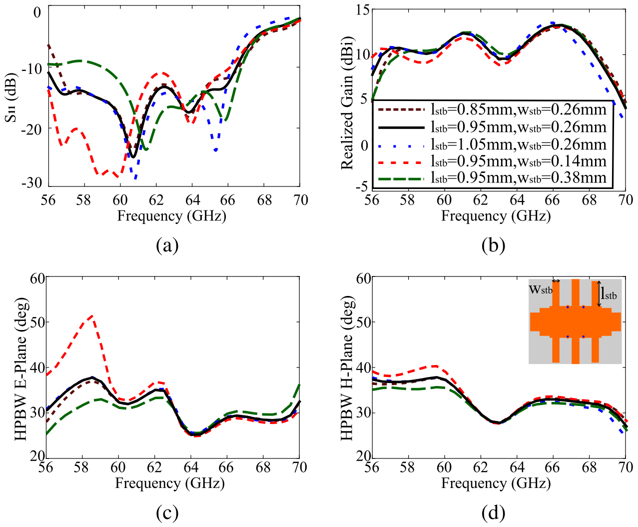

(a) (b) (c) (d)

FIGURE 9. **Simulated $|S_{11}|$, realized gain and half-power beamwidth both along the E-Plane and H-Plane verses the frequency for different tuning stub sizes(l_{stb} and w_{stb}).**

D. TUNING STUBS

Figure 9 illustrates the impact of tuning stub length and width (l_{stb},w_{stb}) on $|S_{11}|$, realized gain, and half-power beamwidth values. Increasing the length l_{stb} value from 0.95 mm to 1.05 mm, shifts both the reflection band and realized gain bandwidth towards the lower frequency range. Notably, the width of the tuning stub (w_{stb}) has a more significant impact on antenna performance compared to the length l_{stb}. As w_{stb} decreases from 0.26 mm to 0.14 mm, the impedance bandwidth extends to lower frequencies, yet the realized gain also shifts downwards, while the half-power beamwidth exceeds 40° along both the planes for frequencies from 56 to 63 GHz. Conversely, increasing w_{stb} beyond the optimal value reduces the half-power beamwidth for both planes for frequencies ranging from 56 to 61 GHz, albeit with $|S_{11}|$ exceeding the -10 dB impedance bandwidth around 58 GHz and a slight reduction in realized gain value. Consequently, $l_{stb} = 0.95$ mm and $w_{stb} = 0.26$ mm are chosen to achieve the widest overlapping impedance/gain bandwidth and half-power beamwidth less than 40° along both the planes.

IV. DIFFERENTIAL FEEDING NETWORK

A. 180° OUT-OF-PHASE SIW POWER DIVIDER

The proposed aperture antenna seamlessly integrates with a differential mm-Wave circuit, eliminating the need for an independent differential feeding network. However, due to the single-ended nature of the existing measurement system, an external balun is required to measure the prototype. Using a balun at such high frequencies is not ideal, as after coupling to the antenna, it causes potential parasitic inductance. This can result in amplitude and phase imbalances, ultimately leading to performance degradation in the proposed prototype.

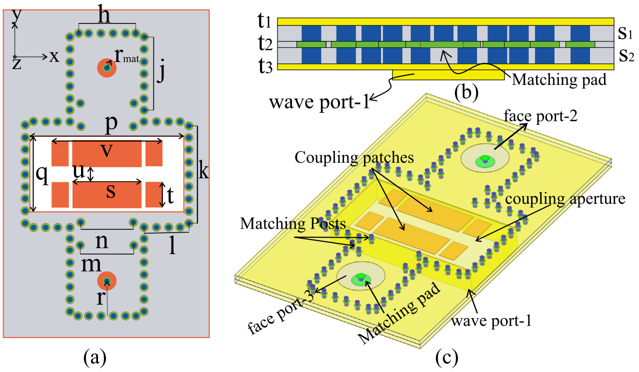

(a) (c)

FIGURE 10. **(a) Top view, (b) Side view and (c) 3-D of 180° out-of-phase SIW power divider. ($h = 1.5$, $j = 1.77$, $k = 2.4$, $l = 1.06$, $m = 1.34$, $n = 1.28$, $p = 3.75$, $q = 1.85$, $r = 0.87$, $s = 1.67$, $t = 0.6$, $u = 0.29$, $v = 2.67$, $r_{mat} = 0.18$) (Units = mm).**

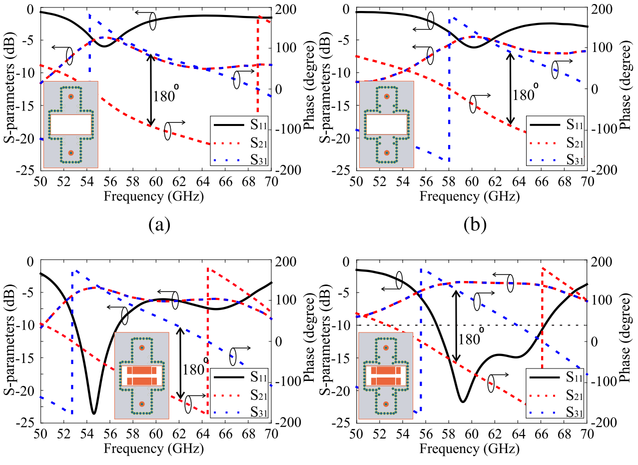

(c) (d)

FIGURE 11. **S-parameters for 180° out of phase SIW power divider. (a) Without the matching posts and coupling patches, (b) only the matching posts exist, (c) only the coupling patches exist, (d) both matching posts and coupling patches exist.**

Although [5], [6] proposed specially designed differential feeding networks integrated with the prototype, they encounter significant issues. These include bulkiness and high substrate loss attributed to the excessive length of the substrate integrated waveguide (SIW) arm. However, inadequate extension of the SIW arms could potentially affect the performance of the prototype. Furthermore the feed network proposed in [5] exhibits asymmetry about the H-plane (i.e., xz-plane), resulting in cross-polarization in the H-plane and asymmetry in the E-plane (i.e., yz-plane) radiation patterns of the prototype.

To address the aforementioned issues, an improved and miniaturized mm-Wave 180° out-of-phase SIW power divider based on an E-plane tee [16] is proposed and depicted in Figure 10(c). Energy is coupled from the WR-15 waveguide to SIW arms using two rectangular coupling patches printed within an aperture on the bottom metal layer. Since the energy is split using an E-plane tee-junction, the energy entering the two SIW arms is inherently of the same magnitude but 180° out-of-phase, resulting in perfectly differential output signals. The SIW arm width is set to 1.66 mm to enable the propagation of only the dominant mode and ensure improved impedance matching. Moreover, two pairs of matching posts are symmetrically positioned at the two outputs of the SIW arms. Subsequently, the energy from the SIW arm is coupled to the signal probe through an SIW-to-probe transition. To ensure optimal impedance matching for this transition, a pair of matching posts is symmetrically placed, accompanied by enlarging the matching pad of the signal via to 0.18 mm. This enlargement mitigates the inductance caused by the signal probe by introducing capacitance perturbation.

The function of coupling patches and matching posts is evident in Figure 11. Without them, as depicted in Figure 11(a), only one resonance at 55 GHz is observed, resulting in poor impedance matching. With the addition of four matching posts, as shown in Figure 11(b), the reflection band shifts downward at higher frequencies. Figure 11(c) demonstrates that introducing rectangular coupling patches enhances impedance matching around 55 GHz and introduces an additional resonance arround 66 GHz. However, the S-parameters are poor at this extra resonance. Thus, optimizing both matching posts and coupling patches is crucial for achieving optimal reflection coefficient at the input port and an acceptable transmission coefficient at the output ports in the proposed 180° out-of-phase SIW power divider.

Following optimization, the detailed design parameters for the proposed 180° out-of-phase power divider are provided in Figure 10(a), along with their values in the caption of Figure 10. Simulated scattering parameters are illustrated in Figure 11(d). We observe that the reflection coefficient of the input port remains below −10 dB, accompanied by a stable insertion loss of less than 0.21 dB from 57 to 66 GHz. The phase difference between the two output ports is approximately 180°, with a negligible phase error of less than 0.06° from 57 to 66 GHz.

B. PROLONG VIA TRANSITION

Considering the intricate fabrication process of LTCC technology based antenna design and measurement setup, eight additional LTCC layers are inserted between the SIW power divider and the antenna part, even though the proposed 180° out-of-phase SIW power divider is only designed on two LTCC layers and can be easily added to the proposed differential antenna to make it single-ended. Figure 12 illustrates the optimized prolonged via transition that feeds energy into the antenna section from the SIW power divider.

The role of circular rings and surrounding vias in the prolonged via transition is illustrated in Figure 13. In Figure 13(a), it's evident that the phase graph is inconsistent in the absence of surrounding vias and circular rings, leading to unacceptable scattering parameters with extremely poor impedance matching at lower frequencies. Conversely, when the signal probe is encircled by vias and

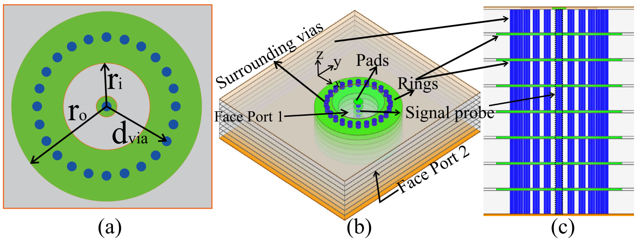

(a) (b) (c)

FIGURE 12. **(a) Top view, (b) 3-D view and (c) Side view of prolong via transition. ($r_i = 0.55$, $r_o = 0.92$, $d_{via} = 0.67$) (Units = mm).**

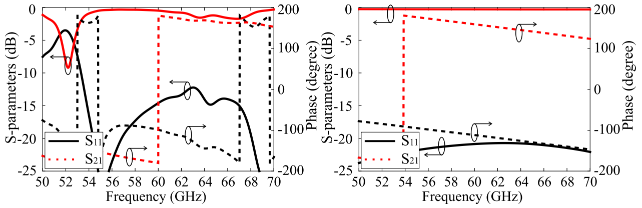

(a) (b)

FIGURE 13. **S-parameters for the prolong via transition. (a) Without the surrounding vias and circular rings and (b) With the surrounding vias and circular rings.**

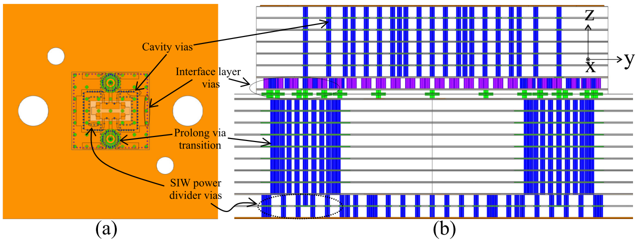

(a) (b)

FIGURE 14. **Proposed differential fed planar aperture antenna. (a) Top view and (b) Side view.**

circular rings, this transition functions similarly to a coaxial cable. The inclusion of surrounding vias and circular rings introduces perturbations in capacitance to counteract the parasitic inductance caused by the signal probe. Figure 13(b) presents the results for the optimized prolonged via transition, where $|S_{11}|$ is less than -20 dB, along with consistent insertion loss of around 0.1 dB. The design parameters for the optimized transition are detailed in Figure 12(a), with their corresponding values provided in the caption of Figure 12.

V. ANTENNA MEASUREMENT

A. SIMULATION AND MEASUREMENT RESULTS

For performance validation, the fabricated antenna prototype depicted in Figure 15(a) is integrated with the SIW differential feeding network shown in Figure 15(c) and connected to a WR-15 waveguide, as illustrated in Figure 15(e). The reflection coefficient of the proposed planar aperture antenna was measured using a mm-Wave network analyzer (Agilent E8364B) with a frequency extension module and a V-band adapter, as depicted in Figure 16(a). Figure 17(a) illustrates a comparison between the simulated and measured reflection coefficients of the proposed antenna. The simulated and measured impedance bandwidths ($|S_{11}| < -10$dB) for the antenna prototype when combined with the differential feeding network are 19.37% (56.55–68.68 GHz) and 20.97% (56.55–69.8 GHz), respectively. Regardless of the integration or disintegration of the differential feeding network, the antenna prototype displays smooth reflection coefficients,

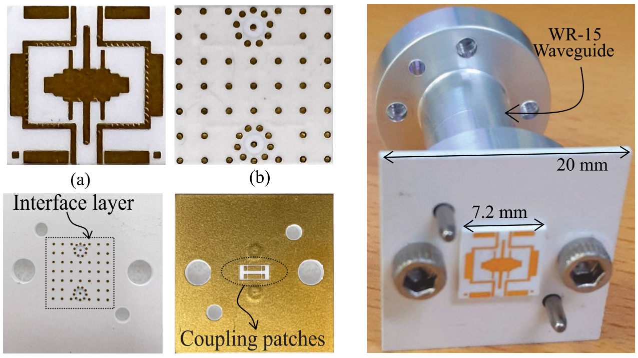

(a) (b) (c) (d) (e)

FIGURE 15. **(a) Top view and (b) Bottom view of fabricated prototype antenna. (c) Top view and (d) Bottom view of fabricated differential feeding network. (e) Fabricated antenna prototype integrated with differential feeding network.**

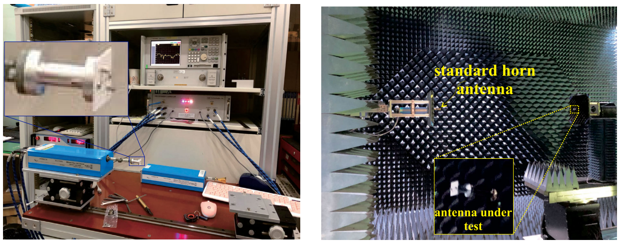

(a) (b)

FIGURE 16. **Antenna under test. (a) Reflection coefficient measurement setup and (b) Far-field measurement setup.**

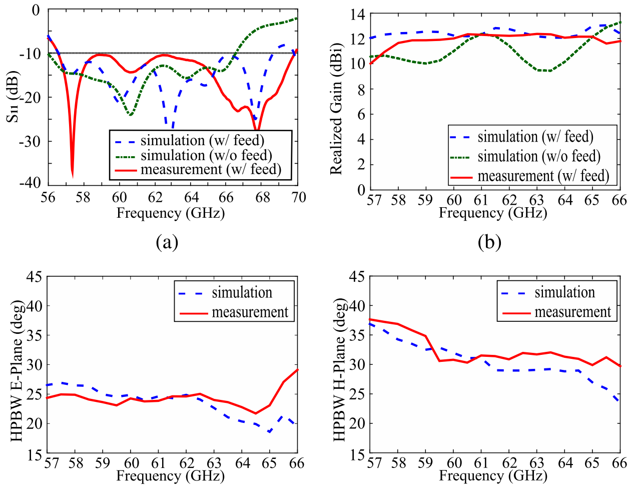

(a) (b)

(c) (d)

FIGURE 17. **Comparison of the simulated and measured results: (a) $|S_{11}|$ (b) Realized gain (c) Half-power beamwidth along the *E*-plane (*yz*-plane) and (d) Half-power beamwidth along the *H*-plane (*xz*-plane).**

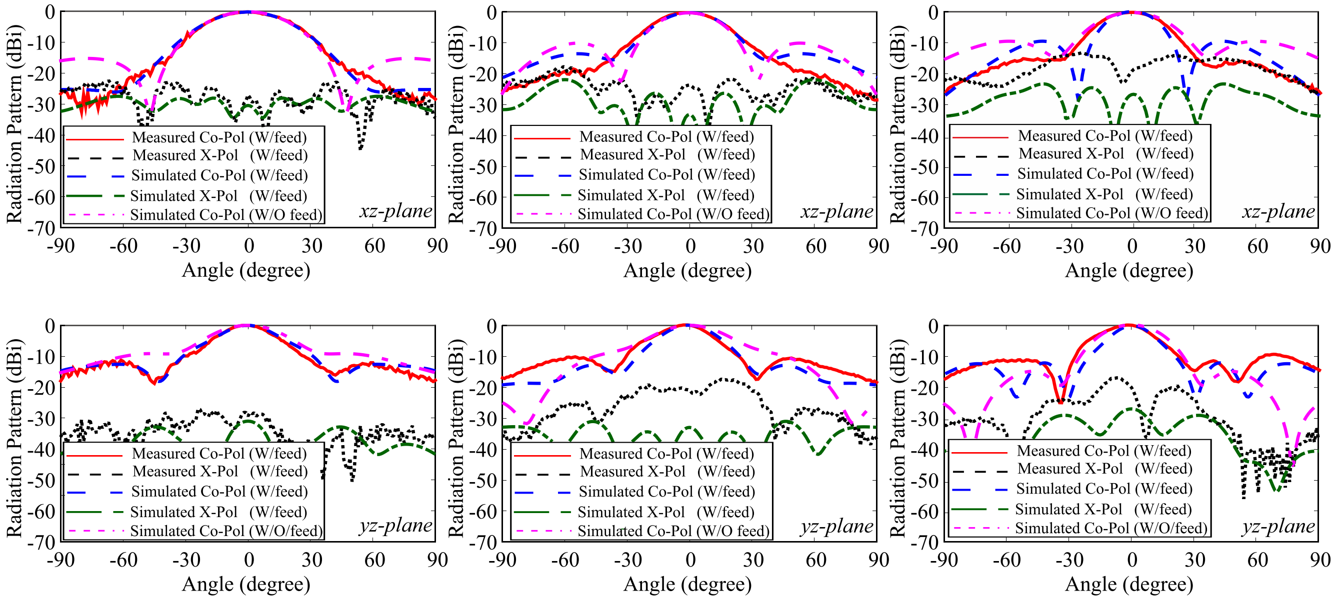

(a) (b) (c)

FIGURE 18. Comparison between simulated and measured normalized co- and cross-polarization both at *H*-plane (*xz*-plane) and *E*-plane (*yz*-plane) (a) 57 GHz (b) 62 GHz and (c) 66 GHz.

TABLE 1. Comparison of various antenna element operating at 60 GHz.

Ref	Antenna Type	Volume (length × width × height) ($\lambda_0{}^3$)	Radiation Aperture (length × width) ($\lambda_0{}^2$)	Impedance Bandwidth	Peak Gain (dBi)	Aperture Efficiency(%) (simulation) (wo feed)	Half-Power Beamwidth (Both Planes)	Radiation Efficiency (simulation) (wo feed)	Technology
[5]	Differenetial-fed Planar Aperture Antenna	–	2.62 × 2.25	21.9 % (56.2 – 69.7 GHz) for $\|S_{11}\| < -10$ dB	15.3	41.2	20 to 30°	$> 85\%$	Single layer laminate
[6]	Differenetial-fed Magnetoelectric dipole antenna	–	1.75 × 1.75	29.2 % (52.6 – 70.6 GHz) for $\|S_{11}\| < -10$ dB	13.7	37.4	40 to 50°	$> 88\%$	Single layer laminate
[7]	Cavity back Magnetoelectric Dipole Antenna	2.21 × 1.27 × 0.125	–	50.6 % (47.5 – 79.5 GHz) for $\|S_{11}\| < -10$ dB	9.1	–	50 to 60°	–	Single layer laminate
[8]	Single-ended-fed planar aperture antenna	3.76 × 4.14 × 0.263	1.41 × 1.41	14.17 % (56.4 – 64.0 GHz) for $\|S_{11}\| < -8$ dB	11.5	46.77	40 to 50°	$> 87\%$	Multilayer LTCC
[9]	Dual polarized planar aperture antenna	2.20 × 2.20 × 0.207	1.39 × 1.39	18.18 % (55.0 – 66.0 GHz) for $\|S_{11}\| < -10$ dB	12	54.57	40 to 50°	$> 85\%$	Multilayer LTCC
Proposed Work	Differential-fed planar aperture antenna	3.77 × 3.77 × 0.393	1.36 × 1.36	20.97 % (56.55 – 69.80 GHz) for $\|S_{11}\| < -10$ dB	12.36	67.47	$< 40°$	$> 85\%$	Multilayer LTCC

λ_0 is the free space wavelength referring to the lowest operating frequency

and no ripples are introduced by the differential feeding network.

The far-field radiation characteristics of the antenna prototype were analyzed in an anechoic chamber utilizing a measurement system specifically designed for mm-Wave antennas, as illustrated in Figure 16(b). A comparison between the simulated and measured broadside gains for the proposed prototype is presented in Figure 17(b). It's evident that the gain form simulation results and measured gain closely align when the antenna is equipped with the differential feeding network, maintaining stability and high gain values compared to the simulated gain without the network. The simulated and measured broadside gain with the feeding network ranges from 12.04 to 13.04 dBi and 10.01 to 12.36 dBi, respectively. The average gain for the prototype antenna integrated with the differential feeding network exceeds that without by 2 dBi, attributed to the increased ground size necessary to connect the antenna to the WR-15 waveguide. In Figure 17(c) and Figure 17(d), both the simulated and measured half-power beamwidth (HPBW) in the *H*-plane (i.e., *xz*-plane) and *E*-plane (i.e., *yz*-plane) remain below 40° across frequencies ranging from 57 to 66 GHz. The discrepancies between simulated and measured results may be attributed to fabrication tolerances and uncertainties. These include variations in the LTCC substrate's permittivity and thickness, metallization losses, and surface roughness in both the antenna and differential feeding parts. Notably, the diameter of the signal probe also plays a significant role.

Figure 18 illustrates the simulated and measured radiation patterns of the antenna prototype integrated with the differential feeding network, alongside the simulated co-polarization of the antenna without the feeding network. These patterns are observed along the H-plane (i.e., xz-plane) as well as along the E-plane (i.e., yz-plane) at frequencies of 57, 62, and 66 GHz. A satisfactory agreement is observed across all three scenarios, achieved by normalizing the radiation patterns using the maximum gain in the respective plane and frequency. Due to the symmetrical structure of the antenna prototype, evident in both configurations with and without the feed network, the co-polarized radiation patterns on the H plane and E plane remain symmetrical, with no significant variations introduced by the feed networks. The simulated and measured broadside cross-polarization level is less than −20 dB for the antenna with the feed network and theoretically zero for the antenna without the feed network. Notably, due to system constraints, radiation patterns were exclusively measured for the upper hemisphere, encompassing the polar angle range [$\theta \in (-90^\circ, 90^\circ)$].

B. COMPARISON WITH PRIOR WORKS

In Table 1, our proposed antenna prototype is compared with various 60 GHz antennas. The planar aperture antenna [5], utilizing differential feeding, offers wide impedance and gain bandwidths. However, despite demonstrating an extremely narrow half-power beamwidth, it lacks compactness compared to our design, featuring a larger physical aperture size and approximately 26% lower aperture efficiency. Similarly, the differentially excited magnetoelectric dipole antenna [6] achieves wide impedance and gain bandwidth but has a wider half-power beamwidth, alongside suffering from a larger aperture size and almost 30% lower aperture efficiency compared to our design. The cavity back magnetoelectric dipole antenna [7] provides a broad impedance bandwidth but has lower gain and wider half-power beamwidth compared to our design. Furthermore, it is unable to benefit from differential microwave circuits. Additionally, all of these designs require complicated differential feeding networks for further extension into an array for high gain.

Leveraging LTCC technology, the single-fed planar aperture antenna [8] offers a compact design but exhibits reduced impedance bandwidth, lower gain, wider half-power beamwidth, and lower aperture efficiency compared to proposed design. Furthermore, it cannot leverage the benefits of differential microwave circuits. In contrast, the differentially excited LTCC-based dual-polarized planar aperture antenna [9] achieves high gain, reaching 12dBi. However, it has a wider half-power beamwidth and lower aperture efficiency compared to the proposed design. Additionally, it necessitates a complex feeding network for array extension.

Our proposed planar aperture antenna stands out due to its compact size, narrowest half-power beamwidth, and highest aperture efficiency. Leveraging both differential feeding and LTCC technology, it is ideal for deployment in mobile environments where multipath interference occurs. It boasts wide impedance and gain bandwidths, higher broadside gain, and maintains half-power beamwidth less than 40° along both planes, ensuring stable radiation patterns and resistance to interference from nearby electromagnetic sources. With these features, our proposed antenna emerges as the optimal choice for AiP mm-Wave applications, offering unmatched efficiency and performance in a compact design.

VI. CONCLUSION

This paper proposes a narrow-beam differentially-fed planar aperture antenna tailored for AiP mm-Wave applications. This antenna not only boasts miniaturization but also offers a wide impedance bandwidth, high gain, narrower half-power beamwidth along both the planes, and low cross-polarization levels with stable radiation patterns. The proposed design features a planar structure with an open cavity enclosing a differentially fed patch, complemented by parasitic strips positioned outside the cavity to narrow the main beam. This feeding approach makes it convenient to integrate with a 60 GHz CMOS differential transceiver chip. The experimental results reveal an impressive −10 dB impedance bandwidth of 20.97% (56.55–69.8 GHz) for the proposed antenna, accompanied by a realized gain ranging from 10.01 to 12.36 dBi. In practical application, the proposed antenna seamlessly integrates with a 60 GHz CMOS differential transceiver chip, obviating the need for a separate differential feeding network. Simulations conducted without the feeding network demonstrate an impedance bandwidth of 17.26% (55.95-66.52 GHz), with a realized gain ranging from 10.56 to 13.28 dBi and a half-power beamwidth less than 40° along both principal cutting planes, showcasing excellent radiation symmetry and polarization purity.

REFERENCES

[1] T. S. Rappaport, R. W. Heath Jr., R. C. Daniels, and J. N. Murdock, *Millimeter Wave Wireless Communications*. London, U.K.: Pearson, 2014.

[2] D. Liu, B. Gaucher, U. Pfeiffer, and J. Grzyb, *Advanced Millimeter-Wave Technologies: Antennas, Packaging and Circuits*. Chichester, U.K.: Wiley, 2009.

[3] S. Esfandiarpour and A. Mallahzadeh, “Wideband planar horn antenna using substrate integrated waveguide technique,” in *Proc. Asia–Pacific Microw. Conf.*, Dec. 2011, pp. 1969–1972.

[4] L. Wang, X. Yin, S. Li, H. Zhao, L. Liu, and M. Zhang, “Phase corrected substrate integrated waveguide H-plane horn antenna with embedded metal-via arrays,” *IEEE Trans. Antennas Propag.*, vol. 62, no. 4, pp. 1854–1861, Apr. 2014.

[5] S. Liao, P. Wu, K. M. Shum, and Q. Xue, “Differentially fed planar aperture antenna with high gain and wide bandwidth for millimeter-wave application,” *IEEE Trans. Antennas Propag.*, vol. 63, no. 3, pp. 966–977, Mar. 2015.

[6] X. Ruan, K. B. Ng, and C. H. Chan, “A differentially fed transmission-line-excited magnetoelectric dipole antenna array for 5G applications,” *IEEE Trans. Antennas Propag.*, vol. 66, no. 10, pp. 5224–5230, Oct. 2018.

[7] J. Zeng and K.-M. Luk, “Single-layered broadband magnetoelectric dipole antenna for new 5G application,” *IEEE Antennas Wireless Propag. Lett.*, vol. 18, pp. 911–915, 2019.

[8] J. Zhu, Y. Yang, S. Li, S. Liao, and Q. Xue, “Single-ended-fed high-gain LTCC planar aperture antenna for 60 GHz antenna-in-package applications,” *IEEE Trans. Antennas Propag.*, vol. 67, no. 8, pp. 5154–5162, Aug. 2019.

[9] S. Liao and Q. Xue, “Dual polarized planar aperture antenna on LTCC for 60-GHz antenna-in-package applications,” *IEEE Trans. Antennas Propag.*, vol. 65, no. 1, pp. 63–70, Jan. 2017.

[10] W. L. Stutzman and G. A. Thiele, *Antenna Theory and Design*, 3rd ed. Hoboken, NJ, USA: Wiley, 2013.

[11] K. F. Lee and K. M. Luk, *Microstrip Patch Antennas*. London, U.K.: Imperial College Press, 2011.

[12] B. Pan, Y. Li, G. E. Ponchak, J. Papapolymerou, and M. M. Tentzeris, "A 60-GHz CPW-fed high-gain and broadband integrated horn antenna," *IEEE Trans. Antennas Propag.*, vol. 57, no. 4, pp. 1050–1056, Apr. 2009.

[13] N. Ghassemi and K. Wu, "Millimeter-wave integrated pyramidal horn antenna made of multilayer printed circuit board (PCB) process," *IEEE Trans. Antennas Propag.*, vol. 60, no. 9, pp. 4432–4435, Sep. 2012.

[14] A. Elboushi and A. Sebak, "High-gain hybrid microstrip/conical horn antenna for MMW applications," *IEEE Antennas Wireless Propag. Lett.*, vol. 11, pp. 129–132, 2012.

[15] A. Enayati, G. A. E. Vandenbosch, and W. De Raedt, "Millimeter-wave horn-type antenna-in-package solution fabricated in a teflon-based multilayer PCB technology," *IEEE Trans. Antennas Propag.*, vol. 61, no. 4, pp. 1581–1590, Apr. 2013.

[16] A. S. Khan, *Microwave Engineering: Concepts and Fundamentals*. Boca Raton, FL, USA: CRC Press, 2014, ch. 3.

[17] T. V. Trinh, S. Trinh-Van, K.-Y. Lee, Y. Yang, and K. C. Hwang, "Design of a low-cost, low-sidelobe-level, differential-fed SIW slot array antenna with zero beam squint," *Appl. Sci.*, vol. 12, no. 21, p. 10826, Oct. 2022.

[18] K.-S. Chin, J.-A. Liu, C. C. Chang, and J.-C. Cheng, "LTCC differential-fed patch antennas with rat-race feeding structures," *Prog. Electromagn. Res. C*, vol. 32, pp. 95–108, 2012.

[19] H. Chu, Y.-X. Guo, and Z. Wang, "60-GHz LTCC wideband vertical off-center dipole antenna and arrays," *IEEE Trans. Antennas Propag.*, vol. 61, no. 1, pp. 153–161, Jan. 2013.

[20] D. Liu and Y. P. Zhang, "Integration of array antennas in chip package for 60-GHz radios," *Proc. IEEE*, vol. 100, no. 7, pp. 2364–2371, Jul. 2012.

[21] D. G. Kam, D. Liu, A. Natarajan, S. Reynolds, H.-C. Chen, and B. A. Floyd, "LTCC packages with embedded phased-array antennas for 60 GHz communications," *IEEE Microw. Wireless Compon. Lett.*, vol. 21, no. 3, pp. 142–144, Mar. 2011.

[22] D. G. Kam, D. Liu, A. Natarajan, S. Reynolds, H.-C. Chen, and B. A. Floyd, "LTCC packages with embedded phased-array antennas for 60 GHz communications," *IEEE Trans. Compon., Packag., Manuf. Technol.*, vol. 1, no. 11, pp. 1806–1814, Nov. 2011.

MUHAMMAD ADNAN was born in Peshawar, Pakistan, in 1996. He received the B.Sc. degree in electrical engineering (major communication) from the University of Engineering and Technology Peshawar, Pakistan, in 2019. He is currently pursuing the combined M.S. and Ph.D. degree in electrical and computer engineering with Sungkyunkwan University, Suwon, South Korea.

His research interests include V-band antenna design, low-temperature co-fired ceramics, shared aperture antenna, and phased array antenna design.

TAEYONG JEONG was born in Iksan, South Korea, in 1991. He received the B.S. degree from the Department of Radio Science Engineering, Chungnam National University, Daejeon, South Korea, in 2018. He is currently pursuing the joint M.S. and Ph.D. degree with the Department of Electronic and Electrical Engineering, Sungkyunkwan University, Suwon, South Korea.

His current research interests include the design of array antenna and optimization algorithms.

JONGJIN PARK received the B.S. and M.S. degrees in electronics engineering and electrical and system engineering from Jeonbuk National University, Jeonbuk, South Korea, in 1999 and 2010, respectively, and the degree in information technology convergence engineering from Pohang University of Science and Technology (POSTECH), Pohang, Gyeongbuk, South Korea, in 2017. From 2010 to 2018, he was a Chief Research Engineer with IMTech, Paju, South Korea, where he was involved in the development of a multi-band antenna and multi-band FEM module, and a dual-band power amplifier module for smartphones. In 2019, he joined AOT Korea Company Ltd., Seoul, South Korea, where he is currently the Research Director. His current research interest includes the design of near-distance high-speed communication module design using a 60 GHz V-band that can replace wired connectors with 60 GHz module technology.

YOUNGOO YANG (Senior Member, IEEE) was born in South Korea, in 1969. He received the Ph.D. degree in electrical and electronic engineering from Pohang University of Science and Technology (Postech), Pohang, South Korea, in 2002. From 2002 to 2005, he was with Skyworks Solutions Inc., Newbury Park, CA, USA, where he designed power amplifiers for various cellular handsets. Since March 2005, he has been with the School of Information and Communication Engineering, Sungkyunkwan University, Suwon, South Korea, where he is currently a Professor. His research interests include RF/mm-wave power amplifiers, RF transmitters, and dc–dc converters.

KANG-YOON LEE (Senior Member, IEEE) received the B.S., M.S., and Ph.D. degrees from the School of Electrical Engineering, Seoul National University, Seoul, South Korea, in 1996, 1998, and 2003, respectively. From 2003 to 2005, he was with GCT Semiconductor Inc., San Jose, CA, USA, where he was the Manager of the Analog Division and worked on the design of CMOS frequency synthesizer for CDMA/PCS/PDC and single-chip CMOS RF chip sets for W-CDMA, WLAN, and PHS. From 2005 to 2011, he was with the Department of Electronics Engineering, Konkuk University, as an Associate Professor. Since 2012, he has been with the School of Information and Communication Engineering, Sungkyunkwan University, where he is currently an Associate Professor. His research interests include the implementation of power integrated circuits, CMOS RF transceivers, analog integrated circuits, and analog/digital mixed-mode VLSI system design.

KEUM CHEOL HWANG (Senior Member, IEEE) received the B.S. degree in electronics engineering from Pusan National University, Busan, South Korea, in 2001, and the M.S. and Ph.D. degrees in electrical and electronic engineering from Korea Advanced Institute of Science and Technology (KAIST), Daejeon, South Korea, in 2003 and 2006, respectively.

From 2006 to 2008, he was with Samsung Thales, Yongin, South Korea, where he was involved in the development of various antennas for wireless communication and radar systems. From 2008 to 2014, he was an Associate Professor with the Division of Electronics and Electrical Engineering, Dongguk University, Seoul, South Korea. In 2015, he joined the Department of Electrical and Computer Engineering, Sungkyunkwan University, Suwon, South Korea, where he is currently a Professor. His research interests include advanced electromagnetic scattering and radiation theory and applications, the design of multi-band/broadband array antennas, and optimization algorithms for electromagnetic applications. He is a Life Member of KIEES and a member of IEICE.

• • •